Journal of Critical Reviews

ISSN- 2394-5125 Vol 7, Issue 1, 2020

Review Article

THERMOLUMINESCENCE CHARCTERISTICS STUDIES OF PHOSPHOR MATERIAL WITH ANTI-BACTERIAL ACTIVITY

P. Rubalajyothi[1], A.Rajendran[1*]

[1]Department of Physics, Nehru Memorial College (autonomous) and affiliated to Bharathidasan University, Puthanampatti, Tiruchirappalli-07, Tamilnadu, India.
***Corresponding Author: neelrajnmc@gmail.com**

Received: 10.11.2019 ***Revised: 16.12.2019*** ***Accepted: 17.01.2020***

ABSTRACT

Rarely measured barium calcium sulfate ($Ba_{1-x}Ca_xSO_4$: Dy^{3+}, Er^{3+}) phosphor material in the research and interpretation of lanthanide series. The solution is obtained from the combustion process. The structure of the objects was confirmed bay X-ray analysis. Also to be consistent with the intensity of the refinement scheme to study the benefits of the fit values, its morphological personality was scanned by scanning with electronic microscopy (SEM). Mixed alkaline rare earth substance $Ba_{1-x}Ca_xSO_4$: Dy^{3+}, Er^{3+} are used for the study for Photoluminescence and thermoluminescence. Here I summarize the thermoluminescence properties of dysprosium and erbium the low, high dose response. The frequency factor (s) and activation energy (E) both were calculated by the first and second law, Chen's half-width method.

Key words: Combustion technique, photoluminescence, Thermoluminescence, T_{max}

DOI: http://dx.doi.org/10.31838/jcr.07.01.106

INTRODUCTION

Phosphors must force their importance to their properties in order to retain the energy that is occurring and convert it into significant radiation. This is called as iridescence, which is carried by electronic process due to its proximity to dimensions of contaminating particles or cross-sectional dropping. Investigation of the coordination and outflow properties of a phosphor can improve the understanding of expensive electronic bioaccumulation and thus the structure of new phosphors of useful importance [1].Though the uses are huge and continue to expand, it still pending that ionizing radiation can cause malignant growth and hereditary degeneration [2]. Nevertheless, the evaluation of the area of radiation and the placement of ionizing radiation has become an investigation to continue to expand the importance of assessing the risks and benefits of the presentation.

Hussain et al. [3, 4] Magnesium phosphate is thought to be the reaction of glass thermoluminescence. The polished curves demonstrated two extremes that were subject to the warming rate. Wijapurger et al. [5] analyzed the TL properties of ordinary sand. Also, they considered the top part to be the dosimeter. Bolognan et al. [6] studied the thermo luminescence reaction of conventional fluoride. Its bright peaks were found at 144°C, 119°C and 224 °C Ramos-Bernal et al [7]. Had studied reproduction of the luminous curve is one precious stone and lift. The dosimetry properties of internal-arranged copper doped with lithium borate using the strategy analyzed using El-Faramawi et al. [8].

Thermoluminescence dosimeter (TLD) is commonly incorporated into the medical, personal, and environment of the ionizing radiation zones. Borate glass for the best dosimeter material was taken because of the close tissue proportional coefficient of coating, high heating sound, low liquefaction point and excellent solubility of abnormal earth particles. The host can provide imaginative effects by modifying its electronic, integral (functional bioaccumulation and synergistic function) and morphological (grain value adjustment, surface area enhancement) properties, and more, with appropriate components for the cross-section [11-16]. Now, unusual earth metals are used as dopants for a variety of applications due to the exceptionally conductive, attractive electrochemical and luminescence properties of electronic transitions within 4f biofilms [17–19].

The rare earth sulfates (RE) are measured and used as dosimeters along extraordinary earth particles has long been investigated. A few specimens are $CaSO_4$: Dy, $CaSO_4$: Eu, $CaSO_4$ and P: Tm phosphor is used widely for environmental verification of radiation. This is due to their increased impact on the radiation area and the simplicity of planning, their high impact, soundness, and dosimetry used in many countries. Currently, Thermo-Irradiance Dosimeter materials are used widely for natural radiation monitoring and personal. Madame relies on its likelihood parameters based on normal dosimetry for any TL phosphorus. This has led to a focus on TL discharge [20]. Inspecting the TL shine curves gives the devices liking parameters. For example, the depth of the web (E), the recurrence factor (S), and the demand of the dynamics (b). Different testing methods include, for example, basic elevation (IR) strategy, curve edge fitting techniques, Chen's half-width techniques, warming-rate techniques, isothermal rotation investigation techniques and more. These were developed to determine these parameters from the TL brightness curves.

In the late Mohir et al., Has given some sulfate phosphorus with characters that can be helpful for TL dosimetry for ionizing radiation [21]. In addition to soluble sulfates, a few experiments are on process of mixed RE products. Some mixed antacid RE products are preserved as of late. Of late, we have been exposed to new halo-sulfate phosphors [22-24]. The reason for the paper is the exposure of the serum-activation of $BaCa(SO_4)_2$ phosphor organized by the co-precipitation technique and the depiction of the thermoluminescence (TL) and photoluminescence (PL) properties imprison parameter, For example, the demand for kinetic (B), functional bioenergetics (E) and

recombination factor (S) can be determined by applying the Chen's half-width technique to a dimly illuminated $BaCa(SO_4)_2$: Ce phosphor which acts as a TLD phosphorus.

It has wide application of TL method. For example, the use and treatment of strong state dosimeters in the industry of radiation dissipaters, and the need for a proper TL dosimetry phosphor to have obvious characteristics in dating practices in earliest geography. For example, in a perfect world, a typical fluorescence curve typically had a separate peak with temperatures above 200 °C. The TL reaction, similar to all the energies of ionizing radiation, is seen as having a high linearity of the TL signal with respect to the light, and the high efficiency of the lower limit region, the less dim, and radiation region. Also part of the late lanthanide arrangement is unusual earth-sized base earth sulfate phosphors, and for example $CaSO_4$: Dy and $CaSO_4$: Tm has high TL impact and insignificant shadow applied to environmental and temporal dosimetry [25].

It has been found that composite sulfates establish a type of TL phosphorus with better execution. For example, $K_2Ca_2 (SO_4)_2$: Eu [26], $K_3Na (SO_4)_2$: Eu [27], $Ba_{0.97}Ca_{0.03}SO_4$: Eu [28], $BaSrSO_4$: Eu [29] and $K_2Ca_2(SO_4)_2$: Eu, $K_2Ca_2(SO_4)_2$: Eu, Dy [30] is considered an exceptionally subtle TLD phosphorus. Dysprosium sesquioxide, Dy_2O_3 is a basic highly insoluble and thermally stable material [31]. What's more, it has a high resistivity, large biocompatibility band, and high dielectric constant [32]. Dy_2O_3 emanating from their 4f electrons is one of its kind properties, as are the various practical products that depend on the dysprosium oxides. They are built on the assortment of uses. For example, Dy_2O_3 is used as a photovoltaic and thermoluminescent material [33, 34]. In this way, the Dy_2O_3 value of the nanocrystalline was calculated by applying NaOH rapidly, adapting the present paper, to investigate the use of a homogeneous precipitation technique. The burning, auxiliary, morphological and electrical properties of the purchased solids were similarly investigated.

In the present experiment, mixed base earth sulfate was measured with $Ba_{1-x}Ca_xSO_4$:Er^{3+} and Dy^{3+} phosphorus. And it was programmed using an answer ignition technique. TL reaction of cobalt-60 gamma-ray beams was contemplated. The TL properties of the $Ba_{1-x}Ca_xSO_4$: Er^{3+}, Dy^{3+} phosphors analyzed in this selection include the catalytic adjustment effect, the acute phase brightness curve patterns, the TL impact partial reaction, and the shape. Parameters of gamma - beam fluorescent $Ba_{1-x}Ca_xSO_4$: Dy^{3+}, $Ba_{1-x}Ca_xSO_4$: Er^{3+} phosphors were determined by Chen's half-width strategy. These two types of rare earth products are manufactured in the same state with solution combustion. It is found that the TL response of Er^{3+} is very low when compared to that of Dy^{3+}. Thus $Ba_{1-x}Ca_xSO_4$ catalyzed with Dy^{3+} is used for further TL studies.

2. Experimental Details:

In this work, analytical grade $Ba(NO_3)_2$(Merck), $(Ca(NO_3)_2.4H_2O)$ (Merck), $((NH_4)_2SO_4)$ (Merck), were in used order to prepare the following composition: $Ba_{1-x}Ca_xSO_4$:Dy^{3+},Er^{3+} with the mol% of ((x=0.03, 0.05, 0.07, 0.09)which means barium nitrate and calcium nitrate dehydrate with stoichiometric (1:1ratio) and the Dysprosium and erbium as the same procedure to take the concentrations are increased up to 0.5, 1, 1.5, 2.0. The Thermoluminescence properties of Nanocrystalline $Ba_{1-x}Ca_xSO_4$ doping Dy^{3+}, Er^{3+} 0.5, 1, 1.5, 2.0 powders were successfully prepared by combustion method using citric acid as fuel. The stoichiometric amounts of barium nitrate (Ba $(NO_3)_2$), calcium nitrate (Ca $(NO_3)_2.4H_2O$), ammonium sulfate $((NH_4)_2SO_4)$ were dissolved in an aqueous solution of urea with constant stirring at room temperature. Using the magnetic stirrer with 80°C under maintain the paste level to transfer the quartz crucible with dried at 440°C for 10 min. After collecting the powder from agate motor then subjected to the grain. The integrated Dy^{3+}, Er^{3+} doped $Ba_{1-x}Ca_xSO_4$ powders recognized the stage arrangement by powder x-beam diffraction strategy utilizing an 'X' Perky Expert PANalytical diffractometer utilizing Cu-Kα radiation (λ= 1.54060Å) as source and worked at 40 kV and 30 MA. The example was examined in the 20 extending from 10 to 80° for 2s in the progression check mode.

2.1. Characterization

TL analysis were done by a PC based TL analyzer, type 5p-400 to nucleonic system 10 mg of powder samples were used for TL measurements, to using the gamma chamber was used for irradiating the sample. For Thermoluminescence think about, nucleonic PC driven TLD framework manual thermo luminescence peruser, physically worked, instruments for Thermoluminescence dosimeters estimation was utilized. The record of typical setup of metal plate in TL gleam bends warmed specifically utilizing a temperature developer, DC speaker photomultiplier and the plant volt recorder. Test being presented to beams of gamma at room temperature from the cobalt-60 sources. After the required presentation, TL glow curves were recorded for 10mg of test each time at a warming rate 5^oCs^{-1} for the equivalent and diverse portion. For correlation, gleam bends were additionally recorded and the photoelectron spectra were gathered on Source Gun A = X-Ray014 400um - FG ON (400 µm).

3. Results and discussion

3.1. XPS

The search through A = X-Ray014 was collected at 400µm - FG ON (400 µm) by light gun spectra. XPS experiment of $BaCaSO_4$ investigates the experimental spectra of Er^{3+} powder. Its structure is to consider the essential lines of all the sections shown on the surface layer of the object. Recordings of such spectra, guided by high-spectrum mode licenses are as usual the peaks of electronic components of erbium, barium, calcium, sulfur, and oxygen. An unprecedented earth solvent was put into the study of basic materials. The uniformly extended barium top ($Ba3d_{5/2}$ doubled as $Ba3d_{3/2}$) in the spectra of the established experiments testifies to the redistribution of parts between the volume and the surface in **Fig.1**. This is usually the result of the defect produced and the surface affected by a situation. The study of Ba3d spectra shows externally for examples of barium carbonate ($Ba3d_{5/2}$ at 781 eV and $Ba3d_{3/2}$ at 796eV) $BaCaSO_4$: Er (line $3d_{5/2}$ line at Ba782 eV) [35].

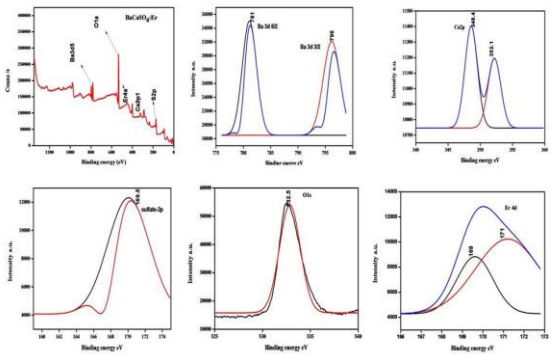

Fig.1. XPS spectra of $BaCaSO_4$ doping rare earth erbium and XPS high resolution spectra of $BaCaSO_4$ doped Er^{3+}.

Calcium oxidation (Ca^{2+}) is the essential constituent of calcium with squares (348.4-352.1 eV) and suggests that it also occurs as $CaHPO_4$, $Ca_3(PO_4)_2$ [36]. The silanized test is undoubtedly an anti-

S2p lubricant, as we can see in the S2p front elevation. Sulfate stabilization is now 169.5eV. We have found that the sulfur 2p excellent can be addressed by a similarly mixed Gaussian line shape and FWHM of 2.79 eV. Controlling XPS Sulfur 2p is mandatory given the weakness of the electronic nature of sulfur inside a particle of oxidized characteristic sulfur. For examples, sulfoxides - (166 eV), sulfones - (168 eV) and sulfonic destruction / sulfate - (169 eV).

Table.1.XPS studies for erbium high resolution spectra.

Thereafter, the de-convolution O1s peak for the O1s spectra is 532.5 ± 0.1 eV. They are excreted to the oxide. In this way, we can observe a lower forced peak at 169-171 eV in the Er 4d region in **table.1**. See also 169-171 eV Er_2O_3 is located in this region [37].

Name	Peak BE	FWHM eV
Ba3d5/2,3/2	781,796	3.35
Ca2p	348.4,352.1	1.38
S2p	169.5	3.07
O1s	532.5	2.55
Er4d	169.82	2.76

3.2.1 Glow curves of Thermoluminescence (TL):

The wide margin of broadest spread utilization of thermo luminescence at present. TL dosimeters should promptly react to gamma radiations. Examination of thermo luminescence shine bends had turned out to be increasingly significant in perspective on its uses in dosimetry, dating and deformity ponder. It demonstrates the run of the mill TL shine bends of $Ba_{1-x}Ca_xSO_4$: Dy^{3+} and Er^{3+} phosphor for the groupings of 0.5mol%, 1mol%, 1.5mol%, and 2 mol%. The shine bends has shown a warming result of $5^oC\ s^{-1}$ and illuminated at a portion rate.

3.2.1.1. TL –Kinetic parameters of Dysprosium:

The gamma chamber shows the radiation injected into the Phosphor object. This means 10Gy to 500Gy with a linear response to the low-level spontaneous emission spectrum. Determination of the best dopants is a significant in planning of a TLD phosphor. Above investigations of the thermo luminescence properties of the Dy coupled $Ba_{1-x}Ca_xSO_4$ test were performed at 1 mol %, catalyst range. From 0·5–2.0 mol%, the $Ba_{1-x}Ca_xSO_4$ tests in **Fig.2** for the conversion of Dy^{3+} amendments were formed by the combustion process. These demonstrate the type of TL force at 119-132 °C tops with Dy^{3+} influence. There is a sustained increase in susceptibility up to 0·5 mol% Dy^{3+}, and from that point on, it decreases somewhat. In this manner, 1.0 mol% Dy^{3+} of $Ba_{1-x}Ca_xSO_4$ can be taken as the best dopants adjustment for the largest yield.

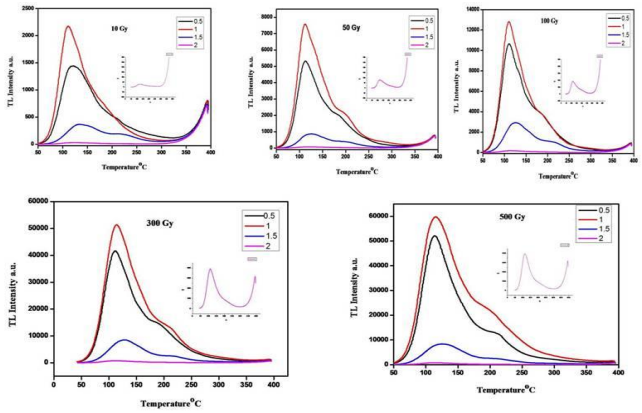

Fig.2. TL glow curves for Dy^{3+}-doped $Ba_{1-x}Ca_xSO_4$ at different gamma doses.

3.2.1.2. Same dose with high response

Insoluble base metals are recorded from the recorded brightness curves for all concentrated abnormal earths. Glacial curves are viewed with a partially moving gamma beam at very intense temperatures in **Fig.3**.

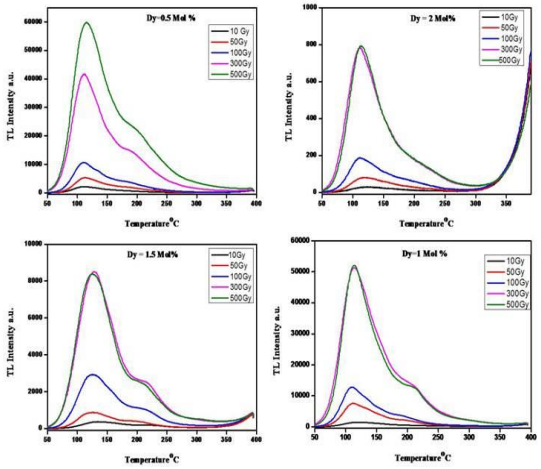

Fig.3. TL glow curves for Dy^{3+}-doped $Ba_{1-x}Ca_xSO_4$ at different gamma doses with Mol%.

This indicates that the individual dimensional brightness of normal depth is related to the surface. The effects of rare earth radiation can speak of two primary wonders: one acting on the general meaning of light. It also focuses on expanding their size and becoming an exciting hotspot for boosting electronics. Likewise, it is caused by the imperfections or the abnormal earth pollution impacts supplied by radiation to lift electrons out of the valence band of matter. The captured electrons re-unite with the residual openings in its filled band during the warming-out phase, giving the hot bright curves.

3.3. Order of kinetics

To using the, formula to followed Chen's peak method to find out the geometry factor, and order of kinetics from that table.

Dose rate(Gy)	Materials /ratio $Ba_{1-x}Ca_xSO_4:Dy^{3+}$	Symmetry factor		Order of kinetics (b)
		Symmetry factor(μg)	Baralin method(γ)	
10Gy	$Ba_{0.97}Ca_{0.03}SO_4:Dy_{0.5}$	0.62	1.7± 0.05	0.62±0.03
	$Ba_{0.95}Ca_{0.05}SO_4:Dy_1$	0.64	2.0±0.01	0.64±0.05
	$Ba_{0.93}Ca_{0.07}SO_4:Dy_{1.5}$	0.47	0.89 ±0.03	0.47±0.03
	$Ba_{0.91}Ca_{0.09}SO_4:Dy_2$	0.63	1.72±0.01	0.63±0.02
Total			1.57±0.05	0.59±0.03
50Gy	$Ba_{0.97}Ca_{0.03}SO_4:Dy_{0.5}$	0.63	1.71±0.02	0.63±0.05
	$Ba_{0.95}Ca_{0.05}SO_4:Dy_1$	0.58	1.38±0.04	0.58±0.04
	$Ba_{0.93}Ca_{0.07}SO_4:Dy_{1.5}$	0.52	1.1±0	0.52±0.03
	$Ba_{0.91}Ca_{0.09}SO_4:Dy_2$	0.59	1.45±0.04	0.59±0.05
Total			1.41±0.01	0.58±0.05
100Gy	$Ba_{0.97}Ca_{0.03}SO_4:Dy_{0.5}$	0.58	1.42±0.05	0.58±0.02
	$Ba_{0.95}Ca_{0.05}SO_4:Dy_1$	0.54	1.17±0.04	0.64±0.04
	$Ba_{0.93}Ca_{0.07}SO_4:Dy_{1.5}$	0.56	1.35±0.05	0.56±0.01
	$Ba_{0.91}Ca_{0.09}SO_4:Dy_2$	0.51	1.07±0.02	0.51±0.05
Total			1.25±0.05	0.57±0.05
300Gy	$Ba_{0.97}Ca_{0.03}SO_4:Dy_{0.5}$	0.54	1.17±0.04	0.54±0.04
	$Ba_{0.95}Ca_{0.05}SO_4:Dy_1$	0.58	1.41±0.06	0.58±0.03
	$Ba_{0.93}Ca_{0.07}SO_4:Dy_{1.5}$	0.59	1.45±0.03	0.59±0.02
	$Ba_{0.91}Ca_{0.09}SO_4:Dy_2$	0.56	1.27±0.07	0.56±0.07
Total			1.32±0.05	0.56±0.05
500Gy	$Ba_{0.97}Ca_{0.03}SO_4:Dy_{0.5}$	0.57	1.35±0.04	0.57±0.05
	$Ba_{0.95}Ca_{0.05}SO_4:Dy_1$	0.57	1.36±0.02	0.57±0.07
	$Ba_{0.93}Ca_{0.07}SO_4:Dy_{1.5}$	0.54	1.19±0.07	0.54±0.05
	$Ba_{0.91}Ca_{0.09}SO_4:Dy_2$	0.58	1.42±0.05	0.58±0.02
Total			1.33±0.01	0.56±0.05

$$\mu g = \frac{\delta}{\omega} \qquad (1)$$

$$E_\tau = \frac{1.51 KT^2 M/\tau - 1.58(2KTm)}{} \qquad (2)$$

$$E_\delta = 0.976 \frac{KT^2 M}{\delta} \qquad (3)$$

$$E_\omega = 2.52 \frac{KT^2 M}{\omega} - 2KTm \qquad (4)$$

$$S = \frac{\beta E}{KT^2 M} \exp \frac{E}{KTm} \ldots \qquad (5)$$

Table.2. Kinetic parameters of *gamma* -ray-irradiated with low dose 10Gy to 500Gy for $Ba_{1-x}Ca_xSO_4:Dy^{3+}$ phosphor calculated from Chen's peak shape method.

Summarizing the characteristic temperatures from the thermoluminescene glow peaks at dose levels of 10Gy to 500 Gy. In **table.2,3** Kinetic order is indicated by the symmetry factor in the last column of table. It was found to have the second-order kinetic in the sample doped with Dy where μ_g is > *0*.50, where as Er^{3+} coupled alkali metals exhibit the 1st order kinetic to increasing the dose level to shift in second order of kinetics for erbium materials. (μ_g < 0.50).

Both maximum peak temperatures and glow curve shape are used for calculating the activation energy .Activation energy thus obtained is slightly different because different basic techniques which were used to produce. The last two methods that of Mazunder et al and Christodoulides are accurate and best also when we equations depending on the total depth.

Dose rate(Gy)	Materials /ratio	τ	δ	ω	E_τ	E_δ	E_ω	E_{avg} (ev)	Frequency factor(s^{-1})
10Gy	$Ba_{0.97}Ca_{0.03}SO_4:Dy_{0.5}$	20	34	54	1.06	0.66	0.8	0.8±0.02	$3.27\pm0.05\times10^{10}$
	$Ba_{0.95}Ca_{0.05}SO_4:Dy_1$	11	23	34	1.9	0.94	1.25	1.35±0.06	$2.97\pm0.02\times10^{17}$
	$Ba_{0.93}Ca_{0.07}SO_4:Dy_{1.5}$	19	17	36	1.20	1.42	1.32	1.31±0.03	$7.91\pm0.03\times10^{15}$
	$Ba_{0.91}Ca_{0.09}SO_4:Dy_2$	25	43	68	0.84	0.53	0.63	0.66±0.06	$5.95\pm0.01\times10^{7}$
50Gy	$Ba_{0.97}Ca_{0.03}SO_4:Dy_{0.5}$	14	24	38	1.52	0.9	1.12	1.18±0.04	$1.32\pm0.04\times10^{15}$
	$Ba_{0.95}Ca_{0.05}SO_4:Dy_1$	13	18	31	1.64	1.21	1.39	1.41±0.03	$1.89\pm0.03\times10^{18}$
	$Ba_{0.93}Ca_{0.07}SO_4:Dy_{1.5}$	20	22	42	1.08	1.04	1.06	1.06±0.04	$1.28\pm0.02\times10^{13}$
	$Ba_{0.91}Ca_{0.09}SO_4:Dy_2$	22	32	54	0.94	0.70	0.79	0.81±0.04	$1.30\pm0.03\times10^{10}$
100Gy	$Ba_{0.97}Ca_{0.03}SO_4:Dy_{0.5}$	14	20	34	1.52	1.09	1.27	1.29±0.03	$3.57\pm0.05\times10^{16}$
	$Ba_{0.95}Ca_{0.05}SO_4:Dy_1$	17	20	37	1.23	1.09	1.16	1.16±0.05	$6.37\pm0.02\times10^{14}$
	$Ba_{0.93}Ca_{0.07}SO_4:Dy_{1.5}$	19	25	44	1.14	0.92	1.01	1.02±0.03	$3.79\pm0.04\times10^{12}$
	$Ba_{0.91}Ca_{0.09}SO_4:Dy_2$	26	28	54	0.79	0.80	0.80	0.80±0.03	$9.36\pm0.04\times10^{9}$
300Gy	$Ba_{0.97}Ca_{0.03}SO_4:Dy_{0.5}$	17	20	37	1.23	1.09	1.16	1.16±0.04	$6.37\pm0.01\times10^{14}$
	$Ba_{0.95}Ca_{0.05}SO_4:Dy_1$	17	24	41	1.23	0.91	1.04	1.06±0.05	$2.85\pm0.03\times10^{13}$
	$Ba_{0.93}Ca_{0.07}SO_4:Dy_{1.5}$	24	35	59	0.88	0.66	0.74	0.76±0.03	$1.31\pm0.04\times10^{9}$
	$Ba_{0.91}Ca_{0.09}SO_4:Dy_2$	18	23	41	1.15	0.95	1.03	1.04±0.03	$1.69\pm0.06\times10^{13}$
500Gy	$Ba_{0.97}Ca_{0.03}SO_4:Dy_{0.5}$	17	23	40	1.24	0.96	1.07	1.09±0.05	$6.53\pm0.05\times10^{13}$
	$Ba_{0.95}Ca_{0.05}SO_4:Dy_1$	19	26	45	1.10	0.85	0.95	0.96±0.06	$3.03\pm0.04\times10^{12}$
	$Ba_{0.93}Ca_{0.07}SO_4:Dy_{1.5}$	26	31	57	0.80	0.74	0.76	0.76±0.06	$5.10\pm0.07\times10^{9}$
	$Ba_{0.91}Ca_{0.09}SO_4:Dy_2$	21	30	51	0.97	0.73	0.82	0.84±0.06	$9.01\pm0.08\times10^{10}$

Table.3. Trapping parameters in $Ba_{1-x}Ca_xSO_4:Dy^{3+}$calculated by Chen's method.

Tmax for Dysprosium

The bio-reaction demonstrates the direct increase of the TL reaction with the expansion of the X-beam biosensor. Because of the high photoluminescence intake coefficient materials for low energy radiation. Dysprosium phosphor was investigated after partial reliability of TL discharge of $Ba_{1-x}Ca_xSO_4$ and fluorescence of phosphor with different amounts of gamma-beams. These demonstrates the TL reaction of 132 °C, the 115°C peak of $Ba_{1-x}Ca_xSO_4$ with the Dy, Er (1 mol %) fraction. The power of the 132 °C, 115°C peak expands directly to an introductory region with a straightforward reaction for higher volumes in **Fig.2**.

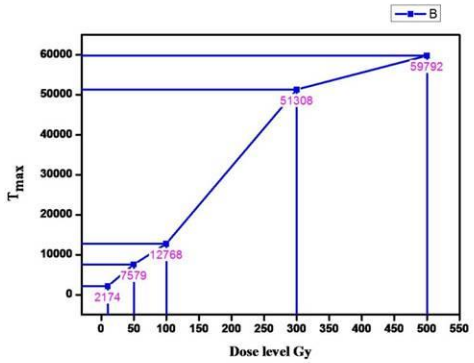

Fig.4. TL dose response for dose level vs. T max intensity with linear response.

The bioactivity of a dosimeter is a significant parameter. Gamma-beams of various energies are used in medical applications. Demonstration applications have high potential in low biomass and restorative applications. A proper dosimeter should act with a similar effect on all energies of radiation in **Fig.4**.

Responsibility of erbium

The result of stiffness and strengthening temperature on thermo luminescence reaction of Dy^{3+} measured with $Ba_{1-x}Ca_xSO_4$ has been extensively investigated. Erbium dope material has been investigated

Dose rate(Gy)	Materials /ratio $Ba_{1-x}Ca_xSO_4:Er^{3+}$	Symmetry factor		Order of kinetics (b)
		Symmetry factor(μg)	Baralin method(γ)	
900Gy	$Ba_{0.97}Ca_{0.03}SO_4:Er_{0.5}$	0.45	0.8± 0.01	0.45±0.01
	$Ba_{0.95}Ca_{0.05}SO_4:Er_1$	0.46	0.85±0.04	0.46±0.03
	$Ba_{0.93}Ca_{0.07}SO_4:Er_{1.5}$	0.41	0.66 ±0.06	0.41±0.01
Total			0.77±0.04	0.44±0.02
1000GY	$Ba_{0.97}Ca_{0.03}SO_4:Er_{0.5}$	0.6	1.8±0.02	0.6±0.03
	$Ba_{0.95}Ca_{0.05}SO_4:Er_1$	0.5	1.25±0.01	0.5±0.05
	$Ba_{0.93}Ca_{0.07}SO_4:Er_{1.5}$	0.54	1.19±0.04	0.54±0.02
Total			1.41±0.04	0.55±0.05
2000Gy	$Ba_{0.97}Ca_{0.03}SO_4:Er_{0.5}$	0.5	1.00±0.01	0.5±0.01
	$Ba_{0.95}Ca_{0.05}SO_4:Er_1$	0.53	1.15±0.01	0.53±0.03
	$Ba_{0.93}Ca_{0.07}SO_4:Er_{1.5}$	0.56	1.31±0.04	0.56±0.01
Total			1.15±0.03	0.53±0.03

Dose rate(Gy)	Materials /ratio	τ	δ	ω	E_τ	E_δ	E_ω	E_{avg} (ev)	Frequency factor(s^{-1})
900Gy	$Ba_{0.97}Ca_{0.03}SO_4:Er_{0.5}$	22	18	40	0.75	0.67	0.71	0.70±0.06	$0.5±0.05x10^9$
	$Ba_{0.95}Ca_{0.05}SO_4$: Er 1	21	18	39	0.78	0.66	0.73	0.72±0.03	$1.14±0.02x10^9$
	$Ba_{0.93}Ca_{0.07}SO_4$: Er 1.5	27	18	45	0.60	0.68	0.64	0.64±0.01	$1.43±0.01x10^{18}$
1000Gy	$Ba_{0.97}Ca_{0.03}SO_4$: Er 0.5	17	31	48	1.16	0.67	0.83	0.88±0.06	$2.09±0.01x10^{11}$
	$Ba_{0.95}Ca_{0.05}SO_4$: Er 1	16	20	36	1.2	1.06	1.15	1.13±0.06	$4.12±0.03x10^{14}$
	$Ba_{0.93}Ca_{0.07}SO_4$: Er 1.5	21	25	46	0.93	0.84	0.88	0.88±0.03	$1.74±0.02x10^{11}$
2000Gy	$Ba_{0.97}Ca_{0.03}SO_4$: Er 0.5	18	18	36	1.10	1.16	1.14	1.13±0.03	$6.07±0.05x10^{15}$
	$Ba_{0.95}Ca_{0.05}SO_4$: Er 1	20	23	43	1.04	0.96	1.00	1.00±0.01	$3.63±0.02x10^{12}$
	$Ba_{0.93}Ca_{0.07}SO_4$: Er 1.5	19	25	44	1.06	0.86	0.94	0.95±0.03	$1.19±0.04x10^{12}$

in the same way that the dysprosium material has been researched using gamma rays. This is no change by low-level radiation.

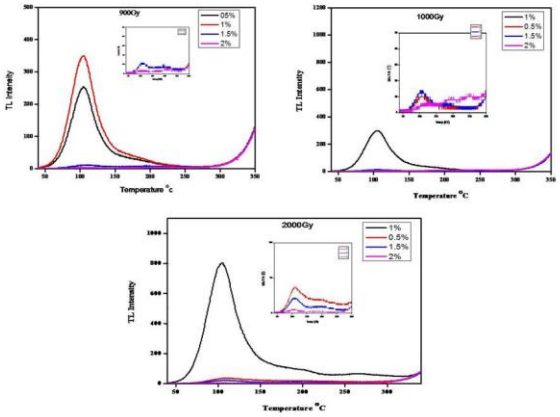

Fig.5. TL glow curves for Er^{3+}-doped $Ba_{1-x}Ca_xSO_4$ at different high gamma doses.

Fig. 5, 6 Compares both Erbium and Dysprosium to the general dysprosium and material folds, which exhibit high levels of radiation. Both the impact of the parameter and the repeating factor with the geometry are valued at the energy demand.

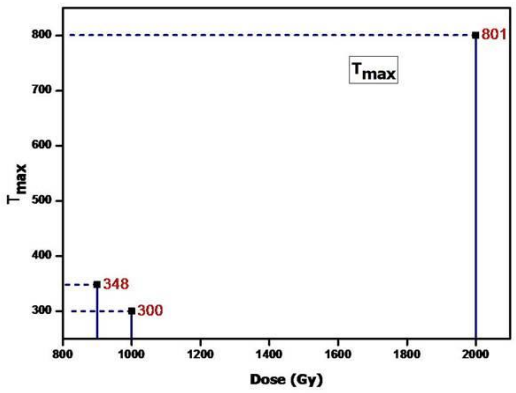

Fig.6. Peak height with dose level as a function of gamma dose for Er^{3+}-doped $Ba_{1-x}Ca_xSO_4$.

If each of the conditions considered in the TL has to be fulfilled, a higher magnitude of low radiation should be given. Figure shows the diffraction and erbium hardening at 440°C at low temperatures for which the TL reaction of $Ba_{1-x}Ca_xSO_4$ is to be calculated in **table.4, 5.**

Table.4. Kinetic parameters of *gamma* -ray-irradiated with high dose 900Gy to 2KGy for $Ba_{1-x}Ca_xSO_4:Er^{3+}$ phosphor calculated from Chen's peak shape method.

Examples are each blinking with gamma beams from 10Gy to 500Gy and 900Gy to 2KGy for TL selection. Examples include the power of high temperature ridges at 107,110 and 115 °C.

Table.5. Trapping parameters in $Ba_{1-x}Ca_xSO_4:Er^{3+}$calculated by Chen's method

Bacteria:

Phosphoric material is naturally present in the film without giving any external dose to kill gram (positive and negative) bacteria. The rare earth substances in chemical compounds in Pseudomonas aeruginosa and ethanol solvents have shown excellent results in **Fig.7**.

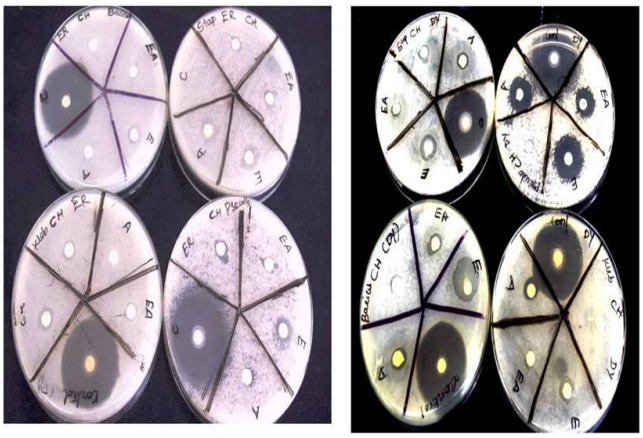

Fig.7. Anti-bacterial activity using different organisms and solvents

Gram-positive and negative (bacteria) are used for various solvents and organisms. As indicated here, a large proportion of Gram-positive and negative microorganisms are capable of killing the infection. The antibacterial exercises of solid and stable water, ethanol, ethyl acetic acid derivative and chloroform use various unusual earth materials as determined by the agar plate dispersion technique. Four other

bacterial pathogens were investigated. For example, Staphylococcus aureus, Klebsiella pneumoniae, Bacillus subtilis, Pseudomonas aeruginosa individually determines various soluble zonal disturbances for use in material testing.

Organisms	**Zone of inhibition (mm)-Erbium**				
	Aqueous	**Ethanol**	**Ethyl acetate**	**Chloroform**	**Control**
Staphylococcus aureus(+)	14	15	9	10	38
Klebsiella pneumoniae	-	11	7	8	35
Bacillus subtilis(+)	10	11	8	9	36
Pseudomonas aeruginosa	10	16	9	10	38

Table.6. Zone of inhibitions recorded against four positive and negative gram bacteria by Using different solvents of erbium

The two different stimulant products for Erbium and Dysprosium in **Table 6, 7** have shown good results for high-intensity Klebsiella pneumoniae of Pseudomonas aeruginosa for the most intense zone control activity. A similar high control of Pseudomonas aeruginosa can be detected in a 15–24 mm zone barrier against Pseudomonas aeruginosa when compared to others, where ethanol is completely soluble.

Organisms	**Zone of inhibition (mm)-Dysprosium**				
	Aqueous	**Ethanol**	**Ethyl acetate**	**Chloroform**	**Control**
Staphylococcus aureus	11	15	8	10	37
Klebsiella pneumoniae	12	13	-	-	35
Bacillus subtilis	12	22	12	-	35
Pseudomonas aeruginosa	20	24	18	-	38

Table.7. Zone of inhibitions recorded against four positive and negative gram bacteria by using different solvents of dysprosium

Compared to the erbium material, this dysprosium material is also found to be more sensitive to bacteria in comparison to the awesome variety. Generic results showed promising model data for the potential employment of ethanol compound enrichment of dysprosium and erbium in the treatment of inevitable life forms.

Conclusion

$Ba_{1-x}Ca_xSO_4$: Er^{3+} and Dy^{3+} phosphor were developed using the combustion method. Dy^{3+}, Er^{3+} doped $Ba_{1-x}Ca_xSO_4$ gamma-room light at low doses, as seen in this article. Erbium has not reached its peak. On the contrary, the high dose, 900Gy to 2KGy, which has a high concentration, showed its sensitivity. I calculated the results by using the same method on 10Gy to 500Gy dysprosium material. With gamma rays injected and its size when blinking, the overlap of all fluorescent ridges proves to be maximal at 500 Gy. Erbium is found in dysprosium with low to very good sensitivity compared to doped products. Erbium measured materials only exhibit high levels of radiation. Peak 1 and 2 peaks have second-order active peaks. Its sensitivity was calculated by using dosimetry characteristics at high and low temperatures. Peak 3 and 4 are the highest in the low temperature location. Subsequently, these peaks are considered suitable for use in high area measurements. Low temperatures are in the 10Gy and 500Gy range. And Erbium is found in the radiotherapy and medical environment from 900Gy to 2KGy. Dysprosium is also sensitive to radiotherapy and medical conditions. Based on that, the estimated value of biomass was estimated to be 0.6 to 1.2 eV and frequency factors from $5.95 \pm 0.01x10^{7}$ to $1.89 \pm 0.03x10^{18}$ and $0.5 \pm 0.05x10^{9}$ to $1.43 \pm 0.01x10^{18}$. And its results were investigated by using gram-positive and different types of bacteria with an anti-agar diffusion method to effectively kill bacteria without any dose.

Acknowledgement

This work is based on the research supported by the RGNF to providing funding agency in UGC and IGCAR from radiological safety division department from Kalpakkam it's helpful to complete in my research work.

References

1. Madhukumar K, Varma HK, Manoj Komath, Elias TS Padmanabhan V and Nair CMK. Photoluminescence and thermoluminescene properties of tri-calcium phosphate phosphors doped with dysprosium and europium. Bull. Mater. Sci. 2007; 30: 527–534.
2. Elkholy MM. Thermoluminescence for Rare-Earths Doped Telluride Glasses. Materials Chemistry and Physics. 2002; 77: 321–330
3. Hussein, A.; Higazy, A.A.; Ewaida, M.A. J. Mater. Sci. 1989, 2, 3371.
4. Hussein A, Higazy A, Sayed AM, Sharaf M and Mansy M. Thermoluminescence response of magnesium phosphate glass to gamma radiation. Radiat. Effects Defects Solids. 1989; 110: 367.
5. Vaijapurkar SG, Raman R and Bhatnagar PK. Sand-a high gamma dose thermoluminescence dosimeter. Radiat. Meas. 1998; 29 (2): 223-226.
6. Balogun, F.A.; Ojo, J.O.; Ogundar, F.O.; Fasasi, M.K.; Hussien, L.A. Radiat. Meas. 1999, 30, 759.
7. Ramos-Bernal S, Negron-Mendoza A and Cruz-Zaragoza E. On the reproducibility of the glow curve of single crystal and commercial LiF. Radiat. Phys. Chem. 2000; 57:735–738.
8. El-Faramawy NA, El-Kameesy SU, El-Agramy A and Metwally G. The dosimetric properties of in-house prepared copper doped lithium borate examined using the TL-technique. Radiation Physics and Chemistry, 2000; 58 (1): 9-13.
9. Jiang LH, Zhang YL and Su Q. Thermoluminescence studies of LiSrBO3:RE3+ (RE = Dy, Tb, Tm and Ce). Appl. Radiat. Isot. 2010; 68: 196 - 200.
10. Hamzah S, Saeed A, Wagiran MA and Hashim IH. Thermoluminescence (TL) dosimeter of dysprosium doped strontium borate glass for different glass modifiers (Na, Li, Ca) subjected from 1 to 9 Gy doses. EPJ Web of Conferences. 2017; 156: 00007.
11. Anita Hastir, Nipin Kohli and Ravi Chand Singh. Comparative study on gas sensing properties of rare earth (Tb, Dy and Er) doped ZnO sensor. Journal of Physics and Chemistry of Solids. 2017; 105: 23–34.

12. Miller DR, Akbar SA, Morris PA. Nanoscale metal oxide-based hetero junctions for gas sensing: A review. Sens. Actuators B. 2014; 204: 250–272.
13. Patil DR, Patil LA and Talanta. Cr_2O_3-modified ZnO thick film resistors as LPG sensors. 2009; 77: 1409–1414.
14. Abhishek Manna, Debasish Sarkar, Shyamaprosad Goswami, Ching Kheng Quah and Hoong-Kun Func. Single excited state intermolecular proton transfer (ESIPT) chemo dosimeter based on rhodol for both Hg^{2+} and OCl^-: ratiometric detection with live-cell imaging. RSC Adv. 2016; 6: 57417.
15. Singh O, Singh RC. Enhancement in ethanol sensing response by surface activation of ZnO with SnO_2. Mater. Res. Bull. 2012; 47(3): 557–561,.
16. C.Y. Tee, G.K. Das, Y. Zhang, T.T.Y. Tan, Pan Stanford Publishing, CRC press, Boca raton, 231–233, (2012).
17. Prospects for rare earth doped GaN lasers on Si, Steckl, J.; Park, J.H.; Zavada, J.M. Mater. Today 2007, 10, 20–27.
18. Vinod Kumar, Ntwaeaborwa OM, Holsa J, Motaung DE and Swart HC. The role of oxygen and titanium related defects on the emission of TiO_2:Tb^{3+} nano-phosphor for blue lighting applications. Optical Materials. 2015; 46: 510–516.
19. Kongre VC, Gedam Sc and Dhoble SJ. Photoluminescence and thermoluminescence characteristics of $BaCa(SO_4)_2$: Ce mixed alkaline earth sulfate. Journal of Luminescence 2013; 135:55-59.
20. Nikhare GN, Gedam SC, Dhoble SJ. Thermoluminescence characteristics of ce^{3+} in halosulphate phosphor synthesized by solid state diffusion reaction. 2018; volume-5:1.
21. Gedam SC, Dhoble SJ, Moharil SV. Synthesis and effect of Ce^{3+} co-doping on photoluminescence characteristics of $KZnSO_4Cl$: M (M= Dy^{3+} or Mn^{2+}) new phosphors,Journal of luminescence 2006; 121 (2):450-455.
22. Gedam SC, Dhoble SJ, Moharil SV. Dy^{3+} and Mn^{2+} emission in KMgSO4Cl phosphor, Journal of luminescence 2007; 124 (1):120-126.
23. Dhoble SJ, Gedam SC, Nagpure IM, Godbole SV, Bhide MK, Moharil SV. Luminescence of Cu^+ in halosulphate phosphor, Journal of materials science 2008; 43 (9):3189-3196.
24. Kongre VC, Gedam SC, Dhoble SJ. Thermoluminescence of γ-irradiated $BaCa\ (SO4)_2$: Eu, Dy, Radiation Effects and Defects in Solids 2015; 170 (7-8):610-620.
25. Pandey S. Bahl K. Sharma R. Ranjan P. Kumar S.P. Lochab V.E. Aleynikov A.G. Molokanov. Thermoluminescence properties of nanocrystalline $K_2Ca_2(SO_4)_3$:Eu irradiated with gamma rays and proton beam, Nucl. Instruments Methods Phys. Res. Sect. B Beam Interact. With Mater. Atoms. 2011; 269:216–222. doi:10.1016/j.nimb.2010.12.005.
26. Dhoble SJ, Mohril SV, Gundu Rao, TK. J. Lumin. 2001, 93, 43.
27. Lochab SP, Sahare PD, Chauhan RS, Salah N, Ranjan R, Pandey A. J. Phys. D: Appl. Phys. 2007; 40:1343.
28. Salah N, Sahare PD, Kumar P. TL and PL in $BaSr(SO_4)_2$:Eu mixed sulphate, phys. stat. solidi (a), 2006: 203: 898.
29. Pandey A, Sharma VK, Mohan D, Kale RK, Sahare PD. Thermoluminescence and photoluminescence characteristics of nanocrystalline $K_2Ca_2(SO_4)_3$: Eu, J. Phys. D: Appl. Phys. 2002; 35(21):2744 ·
30. Sreethawong T, Chavadej S, Ngamsinlapasathian S, Yoshikawa S. A simple route utilizing surfactant-assisted templating sol-gel process for synthesis of mesoporous Dy2O3 nanocrystal. J. Colloid Interface Sci., 2006, 300(1): 219.
31. Pan T-M, Chang W-T, Chiu F-C. Structural properties and electrical characteristics of high-k Dy_2O_3 gate dielectrics. Appl. Surf. Sci., 2011, 257(9): 3964.
32. Chandrasekhar M, Sunitha D V, Dhananjaya N, Nagabhushana H, Sharma S C, Nagabhushana B M, Shivakumara C, Chakradhar R P S. Structural and phase dependent thermo and photoluminescent properties of $Dy(OH)_3$ and Dy_2O_3 nanorods. Mater. Res. Bull., 2012, 47(8): 2085.
33. Chandrasekhar M, Sunitha D V, Dhananjaya N, Nagabhushana H, Sharma S C, Nagabhushana B M, Shivakumara C, Chakradhar R P S. Thermoluminescence response in gamma and UV irradiated Dy_2O_3 nanophosphor. J. Lumin., 2012, 132(7): 1798.
34. Fetisov AV, Kozhina GA, Estemirova S Kh, Fetisov VB, Mitrofanov V Ya, Uporov SA and Vedmid LB. On the room-temperature aging effects in $YBa_2Cu_3O_{6+\delta}$, Journal of Spectroscopy Volume. 2013; 13:217-268.
35. Krzyszt of Rokosz, Tadeusz Hryniewicz, Patrick Chapon, Steinar Raaen and Hugo Ricardo Zschommler Sandim. XPS and GDOES Characterization of Porous Coating Enriched with Copper and Calcium Obtained on Tantalum via Plasma Electrolytic Oxidation, Journal of Spectroscopy Volume. 2016; 7: 709-3071.
36. Khamael M, Abualnaja, Lidija Šiller, Benjamin Horrocks R. Photoluminescence Study of Erbium-Mixed Alkylated Silicon Nanocrystals, World Academy of Science, Engineering and Technology, International Journal of Chemical and Molecular Engineering, 2015; 9:2